Robust Exponential Modulation Integral Observer for Online Detection of the Fundamental and Harmonics in Grid-Connected Power Electronics Equipment

H.S. Lam, Peng Li, Boli Chen, *Member, IEEE*, W.M. Ng, *Member, IEEE*, T. Parisini, *Fellow, IEEE* and
S.Y.R. Hui, *Fellow, IEEE*

Abstract—Harmonic current estimation is required in active power filters for compensation purposes. The most efficient way of calculating the total harmonic current up to the infinite order is to subtract the fundamental component from the distorted current. Direct determination of the fundamental component of a distorted current of mains frequency was realized recently with a 3rd-order modulation integral observer. This paper shows that using an exponential modulation function (Exp-MF) for the integral observer will (i) significantly enhance the robustness of the observer against noise and (ii) automatically remove the low-frequency envelope arising from the D/A and A/C sampling processes compared to previous polynomial modulation function. These new and advantageous features are supported with detailed analysis and experimental verification. The robust observer can be implemented in grid-connected power electronics circuits that require the instantaneous information of the fundamental and/or harmonic currents. Practical comparative tests with the Adaptive Notch Filter and Recursive DFT methods in an active power filter have confirmed the good performance under both steady and dynamic state of the proposed Exp-MF Integral Observer.

Index Terms—fundamental extraction, harmonics detection, active power filters

Nomenclature and Notations

i	line current
i_1, i_k	fundamental current and k^{th} order harmonic current
c	dc current component
a, ω	amplitude and frequency of the fundamental current
y	sum of fundamental current and dc offset
z	state vector of the sinusoidal signal state-space model
T_Δ, T_r	temporal window length and resetting period of the modulation integral observer
t	time variable
t_k	time instant of the kth resetting sequence
d	process disturbance
ϕ_h	general modulation functions, h = 1, 2, 3
$\phi_{p,h}, \phi_{e,h}$	polynomial and exponential modulating functions, h = 1, 2, 3
w_h	weighting parameters of the modulating functions, h = 1, 2, 3
$\Gamma, \Gamma_p, \Gamma_e$	general modulating function matrix and the variants formed by $\phi_{p,h}$ and $\phi_{e,h}$
$v_{\phi,h}$	auxiliary modulated signals

Subscripts, superscripts and accents

$\hat{x}$	estimated signal
$\tilde{x}$	estimation error
x_i	ith component of the vector
$x^{(i)}$	ith order time-derivative of the signal
$x^\top$	transpose

I. INTRODUCTION

THE increasing use of nonlinear loads has prompted the harmonics pollution issues in power systems since the 1980s [1]. The power electronics community responded to this challenge by developing active power (APF) filters [2]-[4] which inject approximate harmonic currents into the ac mains (Fig. 1) in order to comply with various international electromagnetic compatibility (EMC) regulations such as the IEC-61000. A seminal review paper [5] on harmonics detection

H.S. Lam is with the School of Electrical and Electronic Engineering, Nanyang Technological University, Singapore (e-mail: hinsang001@e.ntu.edu.sg).

P. Li. is with the School of Mechanical Engineering and Automation, Harbin Institute of Technology, Shenzhen, China (Email: lipeng2020@hit.edu.cn)

B. Chen is with the Dept. of Electronic and Electrical Engineering at the University College London, London, WC1E 6BT U.K. (e-mail: boli.chen@ucl.ac.uk).

W.M. Ng are with the Dept. of Electrical and Electronic Engineering at the University of Hong Kong, Hong Kong (e-mail: wmng@eee.hku.hk).

T. Parisini is with the Dept. of Electrical and Electronic Engineering at the Imperial College London, London SW7 2AZ, U.K., with the KIOS Research and Innovation Centre of Excellence, University of Cyprus, Nicosia 1678, Cyprus and also with the Dept. of Engineering and Architecture at University of Trieste, TS 34127, Italy. (e-mail: t.parisini@imperial.ac.uk).

S. Y. R. Hui is with the School of Electrical & Electronic Engineering, Nanyang Technological University, Singapore, (e-mail: ron.hui@ntu.edu.sg). He is also with the Department of Electrical &Electronic Engineering, Imperial College London (e-mail: r.hui@imperial.ac.uk).

methods for active power filters was published in 2007. This review paper compares six methods listed as follows: Discrete Fourier Transform (DFT) [6][7], Recursive DFT [8][9], Synchronous Fundamental dq-Frame [10][11], 5th Harmonic dq-Frame [12], p-q Theory [13]; Generalized Integrators. But since its publication, new methods not previously included have been reported. Among them is a modulation integral observer algorithm that adopts a totally different approach [14].

Based on the theoretical work in [14], it is reported in [15] that using Modulation Integrator observer, which determines only the fundamental component of a periodic signal, can be used to obtain the total current harmonic content up to infinite order by simply subtracting the fundamental component from the nonlinear input current. Because such a method can be implemented with a 3rd order observer, it is shown in [15] that it is a fast method with high accuracy. Such an approach is conceptually simple and computationally efficient. It has an advantage of no phase delay between the actual and reconstructed fundamental components of the distorted waveform. Moreover, the proposed method requires only single-phase current measurements for fundamental signal reconstruction. Therefore, it can be easily extended to a three-phase system without being affected by the unbalanced load.

In this paper, the robustness of the modulation integrator observer method against noise and the aliasing issues caused in the A/D and D/A conversion process are explored for practical implementation of the modulation integral observer in a noisy environment. The novel contribution involves the use of a new exponential modulation function (Exp-MF) which can both increase the observer's robustness against noise and eliminate the practical aliasing issues. The mathematical proof on the robustness of the exponential MF over the original MF is included. Practical comparisons of the exponential and the original MF is also provided to confirm the robust performance the exponential modulation integral observer. Finally, the real-

Fig. 1   A typical setup of an Active Power Filter.

time performance of the time-domain Exp-MF method is practically compared with that of the Adaptive Notch Filter (ANF) and frequency-domain Recursive DFT (RDFT) methods

in an active power filter application (Fig. 1).

II. A Summary of the Integral Observer with Polynomial Modulation Function for Detecting the Fundamental Component

This section briefly summarizes the integral observer based on the polynomial modulation function (Fig. 2) that was published in [15]. The line current $i(t)$ is expressed as:

$$i(t) = c + i_1(t) + \sum_{k=2}^{N} i_k(t) \tag{1}$$

where t is the time variable, c is the dc current component, $i_1(t)$ is the fundamental current, $i_k(t)$ is the kth current harmonic component and $\sum_{k=2}^{N} i_k(t)$ is the total harmonic current. Let the fundamental current be:

$$\begin{cases} i_1(t) = a \sin \theta(t) \\ \dot{\theta}(t) = \omega \\ \theta(0) = \varphi \end{cases} \tag{2}$$

and
$$y(t) = c + i_1(t) \tag{3}$$

where a is the amplitude of the fundamental current, ω is the angular frequency, θ is the phase angle and φ is the initial phase angle. The integral observer considers the total harmonic current as "noise" initially. If $y(t)$ can be obtained by the observer, from (1) and (3), the total harmonic current can be obtained easily as follows:

$$\sum_{k=2}^{n} i_k(t) = i(t) - y(t) \tag{4}$$

Therefore, $y(t)$ is chosen to be the single output of the integral. Differentiating (3) twice leads to:

$$y^{(2)}(t) = -\omega^2 i_1(t) \tag{5}$$

where $\ddot{y}(t)$ is the second-order time-derivative of y(t). Based on (3) and (5), one can form the following expression:

$$\begin{bmatrix} y(t) \\ y^{(2)}(t) \end{bmatrix} = \begin{bmatrix} 1 & 1 \\ 0 & -\omega^2 \end{bmatrix} \begin{bmatrix} c \\ i_1(t) \end{bmatrix} \tag{6}$$
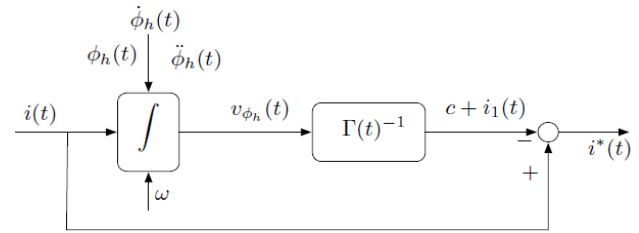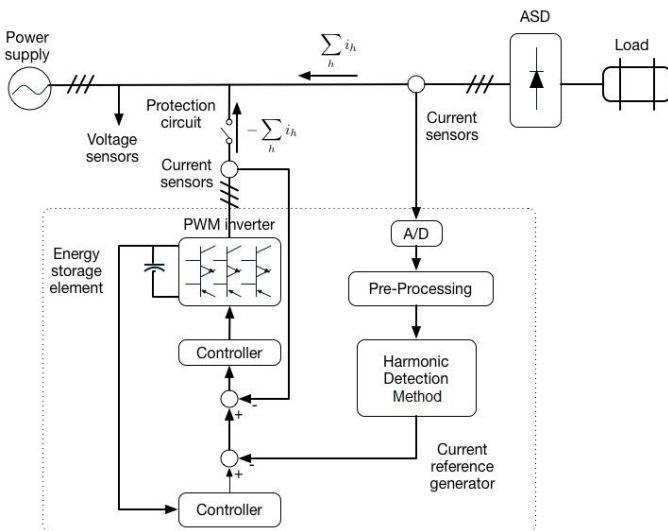

Fig. 2   Block diagram of the MF Integral Observer

As it can be noticed, $y(t)$ can be formulated as the output of a 3rd order state-space observable system:

$$\begin{cases} z^{(1)}(t) = A_z z(t) \\ y(t) = C_z^T z(t) \end{cases} \tag{7}$$

where
$$z(t) = \begin{bmatrix} z_1(t) \\ z_2(t) \\ z_3(t) \end{bmatrix} = \begin{bmatrix} c + a \sin \theta(t) \\ a \omega \cos \theta(t) \\ \omega^2 c \end{bmatrix} \tag{8}$$

$$A_z = \begin{bmatrix} 0 & 1 & 0 \\ -\omega^2 & 0 & 1 \\ 0 & 0 & 0 \end{bmatrix}, C_z = \begin{bmatrix} 1 \\ 0 \\ 0 \end{bmatrix}$$

Since $z_1(t) = y(t)$, the total harmonic current can be derived if $z_1(t)$ is available. In addition, the dc offset and the fundamental component can be individually recovered after simple algebra [6]:

$$\begin{cases} i_1(t) = Gz(t) \\ c = Hz(t) \end{cases} \tag{9}$$

where $G = \begin{bmatrix} 1 & 0 & -\frac{1}{\omega^2} \end{bmatrix}$ and $H = \begin{bmatrix} 0 & 0 & \frac{1}{\omega^2} \end{bmatrix}$.

III. EXISTING POLYNOMIAL MODULATION FUNCTION AND THE PROPOSED EXPONENTIAL MODULATION FUNCTION FOR THE INTEGRAL OBSERVER

In previous works [14][15], a polynomial MF (10) in Table I was used to illustrate the effectiveness of the integral observer in determining the fundamental component. In this paper, we focus on the use of the new exponential MF (11) and compare the performance of these two MFs. As it can be noticed, the exponential MF $\phi_{e,h}(t)$ inherits from the polynomial MF $\phi_{p,h}(t)$ by multiplying an exponentially increasing term $e^{w_h t}$. The purposes of introducing the exponential MF will be illustrated in Section IV.

Table I The Polynomial Modulation Function and the Exponential Modulation Function.

polynomial	exponential
$\phi_{p,h}(t) = \dfrac{w_h t^{2n-h}}{(2n-h)!}$	$\phi_{e,h}(t) = \dfrac{w_h t^{2n-h} e^{w_h t}}{(2n-h)!}$
for $h \in \{1,2,3\}$ (10)	for $h \in \{1,2,3\}$ (11)
The index n is equal to 3 since the fundamental signal is estimated through a 3rd order system (see (7)). w_1, w_2, w_3 are suitable positive weighting factors.	

In the following, we will use $\phi_h(t)$ to denote an unclassified modulation function (which can be either polynomial or exponential). The MFs designed for this application must satisfy two conditions:

1) the MF and its first $(n - 1)$-th derivatives have 0 initial conditions, such that:

$$\phi_h^{(i)}(0) = 0, \quad i = \{0,1,2\} \tag{12}$$

2) The modulation function matrix defined as:

$$\Gamma(t) = \begin{bmatrix} \phi_1^{(2)}(t) & -\phi_1^{(1)}(t) & \phi_1(t) \\ \phi_2^{(2)}(t) & -\phi_2^{(1)}(t) & \phi_2(t) \\ \phi_3^{(2)}(t) & -\phi_3^{(1)}(t) & \phi_3(t) \end{bmatrix}$$

is invertible for any $t \geq t_\epsilon > 0$, where t_ϵ is a small time instant.

Condition 2) can be verified by calculating the determinant of $\Gamma(t)$. For example, with the MFs selected from (10), it is immediate to obtained

$$\det\big(\Gamma(t)\big) = -\frac{w_1 w_2 w_3 t^9}{8640} \neq 0, \ \forall t > 0$$

which implies the invertibility of $\Gamma(t)$. Following the same steps, the invertibility of $\Gamma(t)$ in the context of the exponential MF (see (11)) also can be verified by simple algebras.

With the availability of the modulation function matrix, the following matrix equation can be formed:

$$V_\phi(t) = \Gamma(t)z(t) \tag{13}$$

Hence,

$$z(t) = \Gamma(t)^{-1}V_\phi(t) \tag{14}$$

where the elements of column vector $V_\phi(t) = \begin{bmatrix} v_{\phi 1}(t) & v_{\phi 2}(t) & v_{\phi 3}(t) \end{bmatrix}^T$ can be obtained from the practical measurements of the line current $i(t)$. It follows that,

$$v_{\phi h} = \int_0^t \phi_h^{(3)}(\tau)\, i(\tau) + \omega^2 \phi_h^{(1)}(\tau) i(\tau)\, d\tau \tag{15}$$

To avoid error-accumulation and windup of the pure integrator operator (15) in case the measurement of $i(t)$ is noisy, a periodic resetting strategy is integrated (see Appendix for the derivation of the resetting mechanism [14]). As such, the integral operator (15) is rescaled at time instants t_k, defined as:

$$t_k = T_\Delta + (k + 1)T_r, \ k = 0, 1, 2, \dots \tag{16}$$

where T_r is the period of the resetting scheme, while T_Δ represents the temporal window length of the integration after each rescaling event, $T_r \geq T_\Delta$. When $k = 0$, $t_0 = T_\Delta + T_r$, which represents the first resetting instant. Subsequently, the resetting period is fixed at T_r. In this context, the first derivative of $v_{\phi h}^{(1)}(t)$ can be obtained from the practical measurement of the line current $i(t)$, as follows:

$$v_{\phi h}^{(1)}(t) =$$

$$\begin{cases} \left(\phi_h^{(3)}(t) + \omega^2 \phi_h^{(1)}(t)\right)i(t) & \text{for } 0 \leq t < t_0 \\ \left(\phi_h^{(3)}(t - t_k + T_\Delta) + \omega^2 \phi_h^{(1)}(t - t_k + T_\Delta)\right)i(t) & \text{for } t_k < t \leq t_{k+1} \end{cases} \tag{17}$$

Then, $v_{\phi h}(t)$ can be calculated iteratively, and the value of the modulated signal $v_{\phi h}(t_k)$ at $t = t_k$ is rescaled by

$$v_{\phi h}(t_k) = E_h \Gamma(T_\Delta)\Gamma^{-1}(T_\Delta + T_r)V_\phi(t_k) \text{ for } t = t_k \tag{18}$$

where $E_1 = [1 \ \ 0 \ \ 0], E_2 = [0 \ \ 1 \ \ 0], E_3 = [0 \ \ 0 \ \ 1]$.

The smoothness of the rescaling strategy is justified in the Appendix.

Note that the line current is sampled at a relatively high speed within each repetitive period, and the integral values of (18) can provide the time-domain vector $V_\phi(t)$ continuously at each sampling instant, then the state vector $z(t)$ can be obtained from (14) as

$$z(t) = \begin{cases} \Gamma(t)^{-1}(t)V_\phi(t) & \text{for } t_\varepsilon \leq t \leq t_0 \\ \Gamma(t - t_k + T_\Delta)^{-1}V_\phi(t) & \text{for } t_k < t \leq t_{k+1} \end{cases}$$
(19)

IV. ISSUES IN PRACTICAL IMPLEMENTATION

A. Aliasing issues in A/D and D/A conversion process

In practical implementation, analog-digital (AD) and digital-analog (DA) conversion processes are involved in the sampling of waveforms that tends to introduce additional perturbations to the current signal fed to the observer. A periodic reset of the algorithm (see (17) and (18)) is needed to avoid the accumulation of integral estimation errors. Such processes would lead to an aliasing phenomenon resulting in low-frequency ripples in the envelope of the estimated fundamental component. This section mathematically characterizes the aliasing phenomenon, which is then addressed by the newly developed exponential MF.

To proceed with the analysis, let us consider that the harmonic current signal $i(t)$ is perturbed by a broadband noise $n(t)$. Then, the perturbed signal is expressed as:

$$\hat{i}(t) = i(t) + n(t) = y(t) + n(t) + \sum_{k=2}^{N} i_k(t)$$

where $n(t)$ and the unmodeled high-order harmonics $\sum_{k=2}^{N} i_k(t)$ are treated as the additive disturbance in the estimation scheme. With reference to (17), the noisy input $\hat{i}(t)$ gives rise to a noisy auxiliary signal $\hat{v}_{\phi h}(t)$, as shown by (20) with $d(t) \triangleq n(t) + \sum_{k=2}^{n} i_k(t)$. In contrast to the precise counterpart $v_{\phi h}(t)$ that is driven by $y(t)$, the additive perturbation $d(t)$ leads to an error signal, $\tilde{v}_{\phi h}(t) \triangleq \hat{v}_{\phi h}(t) - v_{\phi h}(t)$, expressed as (21) where $\tilde{v}_{\phi h}(t_k^+) = E_h\Gamma(T_\Delta)\Gamma^{-1}(T_\Delta + T_r)\tilde{V}_\phi(t_k)$ is the rescaled error, depending on the terminal error of previous time interval

$$\tilde{V}_\phi(t_k) = \left[\tilde{v}_{\phi 1}(t_k)\ \tilde{v}_{\phi 2}(t_k)\ \tilde{v}_{\phi 3}(t_k) \right]^T.$$

In view of (19) and (21), the estimation error of $y(t)$, defined by $\tilde{y}(t) \triangleq \hat{y}(t) - y(t)$ takes on the form of (22) with

$$\Phi(t) \triangleq \begin{bmatrix} \phi_1^{(3)}(t) & \phi_1^{(1)}(t) \\ \phi_2^{(3)}(t) & \phi_2^{(1)}(t) \\ \phi_3^{(3)}(t) & \phi_3^{(1)}(t) \end{bmatrix}$$

and

$$\tilde{y}(t_k^+) = E_1\Gamma(t - t_k + T_\Delta)^{-1}\tilde{V}_\phi(t_k^+)$$

is the rescaled terminal error at the end of the previous time-interval. Because of (9), the total error $\tilde{y}(t)$ consists of two parts: the fundamental current estimation error $\tilde{i}_1(t) \triangleq \hat{i}_1(t) - i_1(t) = G\,\tilde{z}(t)$ and the dc offset estimation error $\tilde{c}(t) \triangleq \hat{c}(t) - c = H\,\tilde{z}(t)$, such that $\tilde{i}_1(t) + \tilde{c}(t) = \tilde{y}(t)$.

In view of (22), the integral operator offers satisfactory attenuation of the high frequency components, including the harmonics $\sum_{k=2}^{N} i_k(t)$ and the high frequency contents contained in $n(t)$. However, the remaining low-frequency components, unless being zero-mean and uncorrelated with the modulation function $\Phi(t)$, the error signal $\tilde{y}(t)$ is prone to diverge due to the error accumulation within two continuous resetting instants. In combination with the resetting mechanism that inherently prevents the drift by downscaling the estimation error, the resulting fundamental signal estimates appear as a swinging sinewave. A numerical example is shown in Fig. 3, which is obtained by repeating the simulation example presented in [6] whereas the harmonic current signal is affected by a non-zero mean uniform distributed disturbance.
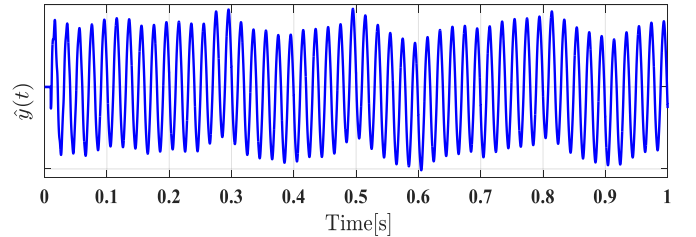

Fig. 3 Reconstructed fundamental signal by the modulation integral observer in the presence of a non-zero mean uniform disturbance.

B. Anti-aliasing solutions

Now, two possible approaches are introduced to reduce the aliasing effect.

$$\hat{v}_{\phi h}^{(1)}(t) = \begin{cases} \left(\phi_h^{(3)}(t) + \omega^2\phi_h^{(1)}(t)\right)\left(y(t) + d(t)\right) & \text{for } 0 \leq t < t_0 \\ \left(\phi_h^{(3)}(t - t_k + T_\Delta) + \omega^2\phi_h^{(1)}(t - t_k + T_\Delta)\right)\left(y(t) + d(t)\right) & \text{for } t_k < t \leq t_{k+1} \end{cases}$$
(20)

$$\tilde{v}_{\phi h}(t) = \begin{cases} \int_0^t \left(\phi_h^{(3)}(\tau) + \omega^2\phi_h^{(1)}(\tau)\right) d(\tau)\,d\tau, & 0 \leq t < t_0, \\ \int_{t_k}^t \left(\phi_h^{(3)}(\tau - t_k + T_\Delta) + \omega^2\phi_h^{(1)}(\tau - t_k + T_\Delta)\right) d(\tau)\,d\tau + \tilde{v}_{\phi h}(t_k^+), & t_k < t \leq t_{k+1}, \end{cases}$$
(21)

$$\tilde{y}(t) = \begin{cases} E_1\Gamma(t)^{-1}\int_0^t \Phi(\tau)\begin{bmatrix} 1 \\ \omega^2 \end{bmatrix} d(\tau)\,d\tau, & 0 \leq t < t_0, \\ E_1\Gamma(t - t_k + T_\Delta)^{-1}\int_{t_k}^t \Phi(\tau - t_k + T_\Delta)\begin{bmatrix} 1 \\ \omega^2 \end{bmatrix} d(\tau) + \tilde{y}(t_k^+), & t_k < t \leq t_{k+1}, \end{cases}$$
(22)

(i)   Pre-filtering of the current signal $i(t)$

It is intuitive to apply a pre-filter to filter out the low-frequency contents in $i(t)$, such that the swing phenomenon can be removed. With the aim of maintaining the amplitude and phase angle of the fundamental signal $i_1(t)$ in the filtered signal, a specialized band-pass filter

$$F(s) = \frac{K_s^2 \omega_s s}{s^2 + K_s \omega_s s + \omega_s^2} \tag{23}$$

is designed with $\omega_s = 2\pi \cdot 50$ and $K_s = 1$.

It is important to note that the gain of the filter F(s) at the fundamental frequency 50Hz is 0dB and the associated phase shift is 0, and consequently the fundamental signal $i_1(t)$ can be accurately estimated by the observer without using any post-correction scheme for the phase and amplitude. The effectiveness of $F(s)$ are illustrated by the same simulation example deployed in the previous section. As shown in Fig. 4, the swing phenomenon is favorably eliminated by adding the band-pass filter to the observer scheme. However, the additional filter slows down the convergence speed at the beginning due to the transient response of the filter, and also increases the overall complexity of the methodology.
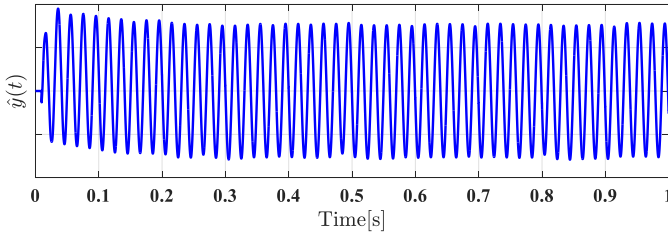

Fig. 4 Reconstructed fundamental signal by the modulation integral observer with the pre-filter in the presence of a non-zero mean uniform disturbance.

(ii)   Exponential modulation function

In this section, it will be shown that the aliasing issue can be addressed by the newly designed exponential MF $\phi_{e,h}(t)$ (see Table I) without using an additional filter, thereby the convergence speed is not compromised.

To proceed with the analysis, let us first recall the MFs selected from (10) and (11):

$$\phi_{p,1}(t) = \frac{w_1 t^5}{5!}, \phi_{p,2}(t) = \frac{w_2 t^4}{4!}, \quad \phi_{p,3}(t) = \frac{w_3 t^3}{3!} \tag{24}$$

$$\phi_{e,1}(t) = e^{w_1 t}\frac{w_1 t^5}{5!}, \qquad \phi_{e,2}(t) = e^{w_2 t}\frac{w_2 t^4}{4!},$$

$$\phi_{e,3}(t) = e^{w_3 t}\frac{w_3 t^3}{3!} \tag{25}$$

In view of (21), the estimation error $\tilde{v}_{\phi h}(t)$ at an arbitrary time instant is composed of two parts: 1) the rescaled terminal error at the end of the previous time-interval (initial error at $t = 0$ is 0), and 2) the accumulated error within the present time-interval. Next, the error comes from 2) will be investigated first whereas the error signal 1) will be studied later.

Without loss of generality, let us pick the first time-interval $t \in [0, t_0]$. In the context of the polynomial case, the estimation error $\tilde{v}_{\phi p1}(t)$ induced by $\phi_{p,1}(t)$ can be evaluated by:

$$\tilde{v}_{\phi p1}(t) = \int_0^t \left(\phi_{p,1}^{(3)}(\tau) + \omega^2 \phi_{p,2}^{(1)}(\tau) \right) d(\tau)\, d\tau$$

$$= \int_0^t \left(\frac{w_1 \tau^2}{2!} + \omega^2 \frac{w_1 \tau^4}{4!} \right) d(\tau)\, d\tau \tag{26}$$

Assuming that $d(t)$ is a periodic signal formed by M sinusoidal components, $d_1, d_2, \cdots, d_M$ with associated frequencies $\omega_{d_1}, \omega_{d_2}, \cdots, \omega_{d_M}$. Due to the linearity of the integral operator, the error term $\tilde{v}_{\phi p1}(t)$ can be expressed as the sum of M components $\tilde{v}_{\phi p1,1}(t), \tilde{v}_{\phi p1,2}(t), \cdots, \tilde{v}_{\phi p1,M}(t)$ induced by each individual component of $d(t)$, respectively. Therefore, with reference to (26) it holds that

$$\tilde{v}_{\phi p1,i}(s) = w_1 s \left[\frac{1}{2}\left(\frac{d^2}{ds^2}\frac{\omega_{d_i}}{s^2 + \omega_{d_i}^2} \right) \right.$$
$$\left. + \frac{\omega^2}{24}\left(\frac{d^4}{ds^4}\frac{\omega_{d_i}}{s^2 + \omega_{d_i}^2} \right) \right] \tag{27}$$

where $i = 1,2, \ldots, M$, s is the Laplace variable. After some algebra, we obtain

$$\tilde{v}_{\phi p1,i}(s) = G_{p1,i}(s)d_i(s), \quad i = 1,2, \ldots, M \tag{28}$$

where

$$G_{p1,i}(s) = s\frac{w_1}{2}\left(\frac{8s^2}{\left(s^2 + \omega_{d_i}^2\right)^2} - \frac{2}{s^2 + \omega_{d_i}^2} \right)$$

$$+ s\frac{\omega^2 w_1}{24}\left(\frac{384 s^4}{\left(s^2 + \omega_{d_i}^2\right)^4} - \frac{288 s^2}{\left(s^2 + \omega_{d_i}^2\right)^3} + \frac{24}{\left(s^2 + \omega_{d_i}^2\right)^2} \right).$$

As it can be noticed, the sensitivity function of system (28) (that is $\left|1 - G_{p1,i}(j\omega)\right|$) has the sensitivity peak at ω_{d_i} since the closed-loop transfer function $G_{p1,i}(s)$ is characterized by imaginary poles at $\pm j\omega_{d_i}$. Therefore, the system (28) is sensitive to $d_i(t)$, which also implies that $\tilde{v}_{\phi p1}(t)$ is sensitive to all frequency components. Analogously, it can be inferred that $\tilde{v}_{\phi p2}(t)$ and $\tilde{v}_{\phi p3}(t)$ are also sensitive to periodic disturbances when polynomial MFs (24) are applied.

By analogy to (26), the error term $\tilde{v}_{\phi 1}(t)$ driven by the exponential MF $\phi_{e,1}(t)$ is expressed as (29), with $p_2 = 1, p_3 = 2, p_4 = 3, p_5 = 4, q_1 = 1, q_5 = 2, \alpha_2 = 2, \alpha_3 = 2, \alpha_4 = 8, \alpha_5 = 120, \beta_4 = 24, \beta_5 = 120$. By following the same steps (27)-(28) taken in the polynomial case, we have

$$\tilde{v}_{\phi e1,i}(s) = G_{e1,i}(s)d_i(s), \quad i = 1,2, \ldots, M \tag{30}$$

where $G_{e1,i}(s)$ is the transfer function induced by exponential MFs. Due to the exponential term $e^{w_1 t}$, all the imaginary poles at $\pm j\omega_{d_i}$ are shifted to the right-hand side of the complex plane by w_1, such that the new poles are $w_1 \pm j\omega_{d_i}$. In this context,

$$\tilde{v}_{\phi e1}(t) = \int_0^t \left(e^{w_1\tau}\left(\frac{w_1^4\tau^5}{120} + \frac{w_1^3\tau^4}{8} + \frac{w_1^2\tau^3}{2} + \frac{w_1\tau^2}{2} + \omega^2\left(\frac{w_1^2\tau^5}{120} + \frac{w_1\tau^4}{24} \right) \right) \right) d(\tau)\,d\tau$$

$$= \int_0^t \left(e^{w_1\tau}\left(\sum_{i=2}^5 \frac{w_1^{p_i}\tau^i}{\alpha_i} + \omega^2\left(\sum_{i=4}^5 \frac{w_1^{q_i}\tau^i}{\beta_i} \right) \right) \right) d(\tau)\,d\tau \tag{29}$$

the sensitivity to sinusoidal disturbances, d_i, $i = 1,2,\dots,M$, is significantly reduced. For the sake of completeness, the bode plots of $G_{p1,i}(s)$, $G_{e1,i}(s)$ with $w_1 = 45$ and $\omega_{d_i} = 5\,\text{Hz}$ are depicted in Fig. 5 as an illustrative example. As it can be seen, the sensitivity peak appears in $G_{p1,i}(s)$ is effectively removed in the exponential counterpart $G_{e1,i}(s)$.
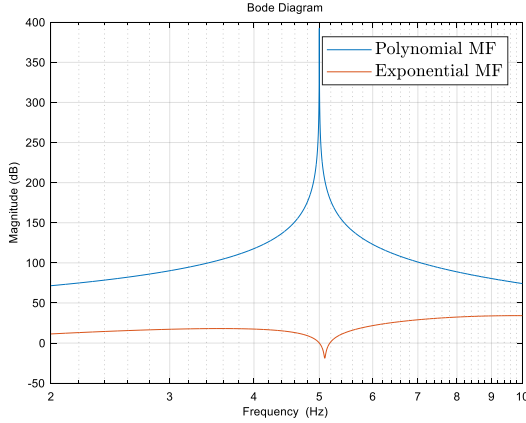
Fig. 5 Bode diagram of the transfer functions $G_{p1,i}(s)$, $G_{e1,i}(s)$ with $w_1 = 45$ and $\omega_{d_i} = 5\text{Hz}$.

Although closed-loop transfer functions $G_{p1,i}(s)$, $G_{e1,i}(s)$ in both cases are not stable (because of multiple 0 poles in the polynomial case and poles with positive real parts in the exponential case), the divergence of the estimation error $\tilde{v}_{\phi 1,i}(s)$ evoked by the unstable poles (introduced by on the polynomial and exponential functions, respectively) are highly attenuated in $\tilde{y}(t)$ by the MF matrix $\Gamma(t)^{-1}$ as the rates of the divergence are compensated by the rate of decay (i.e., $\Gamma(t)^{-1}$ formed by the same type of MFs in each case). Finally, the boundedness of the $\tilde{y}(t)$ is rigorously ensured by the resetting mechanism with the properly selected T_Δ, T_r, and the observer scheme is subject to Input-to-State stability [15]. Generality speaking, the algorithm has to be reset frequently enough to avoid error accumulation and thereby to ensure stability.

Next, the initial error (rescaled terminal error at the end of the previous time-interval) at each time-interval will be studied. Let us start by demonstrating that the rescaling gain of the exponential MFs is much smaller than the one induced by the polynomial MFs for possible choices of T_Δ and T_r around 0.1s (which is selected for both resetting coefficients in [6]). Let us consider the norm of the rescaling gains in both cases

$$\gamma_i \triangleq \left| \Gamma_i(T_\Delta)\Gamma_i(T_\Delta + T_r)^{-1} \right|, i = \{p, e\}$$

where Γ_p and Γ_e represent the MF matrix formed by polynomial and exponential MFs, respectively. The map of the ratio γ_p / γ_e with respect to T_Δ and T_r is illustrated in Fig. 6,

where the benefit of exponential MFs in terms of scaling down the gain is clearly presented. As such, the rescaled error of the exponential MFs at each resetting instant tends to be smaller as compared to the polynomial counterparts by also considering the noise sensitivity in both scenarios.

Now, it is possible to infer from the analysis that the robustness of the modulation integral observer is expected to be improved by replacing the polynomial MFs with the exponential ones. Thus, the swing phenomenon tends to be suppressed without adding an extra filter, which will be experimentally verified in Section IV.
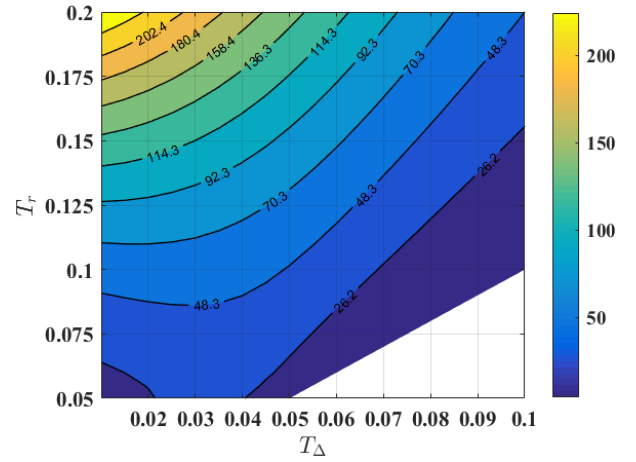

Fig. 6 Ratio between norms of rescaling gains induced by both MFs with respect to T_Δ and T_r. (Both types of MFs have same parameter settings: $w_1 = 45$, $w_2 = 35$, $w_3 = 15$).

V. PRACTICAL IMPLEMENTATION AND EVAULATION

Four sets of practical tests have been conducted to evaluate the performance of the proposed method. First, the robustness of the exponential and the polynomial modulation functions are compared under different noise levels. Second, a comparison of the computation time between polynomial and exponential modulation on FPGA and microcontroller is evaluated. Third, the practical implementation of the exponential modulation in an active power filter is demonstrated in a hardware setup. Finally, the dynamic performance has been compared between RDFT and Exp-MF.

A　Comparison of the exponential and polynomial modulation functions for the integral observer

Practical tests have been conducted to compare the performance of the two MFs under noiseless and noisy situations. The reference waveform used in this test is shown in Fig. 7 and its harmonic content is tabulated in Table II. Note

that this reference waveform is based on the example (with the same relative harmonic ratios) used in the comparison in [5] for a range of harmonic detection methods. The third harmonic is not included because it is cancelled in a 3-phase power system with a delta-connected transformer. In the experiment, the weighted coefficients w_1, w_2, w_3 are selected as 45, 35 and 15 for both polynomial and exponential MFs. The fundamental rule for tuning w_1, w_2, w_3 is to minimize the condition number of $\Gamma(t)$, in order to render feasible the practical inversion of $\Gamma(t)$, in the interval $[t_\epsilon, T_\Delta + T_r]$. Note that the inverse matrix $\Gamma(t)^{-1}$ can be computed analytically once the MFs have been chosen, thereby the inverse can be implemented directly, to avoid online matrix inversion. The noise used for the practical tests is the Gaussian white noise and the peak to peak magnitude of the noise is set at 0.26V, 1V, 2V, and 3V. The reset time is $T_\Delta = T_r = 0.1$ s and the sampling frequency is 10kHz.The harmonic current and the noise are generated by the function generator Tektronix AFG3102C and the algorithm is implemented by dSPACE DS1006.
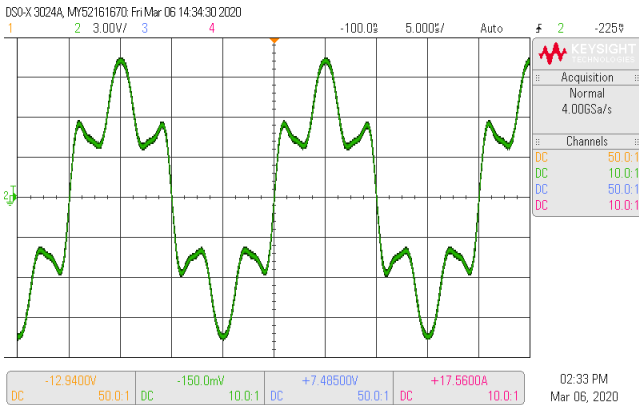
Fig. 7 Practical periodic distorted waveform for evaluation of fundamental detection algorithm

Table II   Fundamental and harmonic content to reference waveform

Fundamental/Harmonic	Voltage (V)
dc offset	0
Fundamental	7.8
5th harmonic	2.25
7th harmonic	0.39
11th harmonic	0.39
13th harmonic	0.39

The error is calculated by the following method. First a pre-designed harmonic current and fundamental current are injected by a functional generator to the dSPACE. Also, a fundamental current is injected to the dSPACE at the same time. Hence, the reconstructed fundamental current will be subtracted by the injected fundamental current in the program and output by the digital-to-analog converter (DAC) to the scope and further analysis can be carried out by capturing the data. The method used here is to eliminate the phase error between the reconstructed and injected fundamental current as the functional generator can provide the two signals that are perfectly in phase.

Fig. 8a to Fig. 8c show the actual and reconstructed fundamental waveforms by the polynomial MF integral observer under noiseless and different noisy conditions. The corresponding measurements for the exponential MF integral observer are shown in Fig. 9a to Fig. 9c. It can be seen from Fig. 8a to Fig. 8c that the polynomial MF integral observer can estimate the fundamental component accurately when there is no noise. But the quality of the reconstructed fundamental waveform deteriorates with the increasing noise level. The reconstructed fundamental is affected by the noise and suffers from a swing issue. Therefore, the results are highly affected. However, the reconstructed fundamental waveforms using the exponential MF integral observer are relatively closer to their ideal sinusoidal references with no obvious swing phenomena.

An alternative way to observe the robustness against noise is to plot the error-time series. Such results under different noise conditions (noise level of 0V, 2V and 3V) are plotted in Fig. 10a-Fig. 10c. In all cases, the exponential MF has less error and outperforms the polynomial MF. These practical results confirm that the exponential MF integral observer has more robustness against noise than the polynomial counterpart. These waveforms are further analyzed so that their root-mean-square (RMS) error and error boundary (which is the maximum error minus the minimum error) are obtained. Table III shows the RMS error and the error boundary for both MFs.

B.   Comparison of computational times of online implementations in microcontroller and FPGA

The previous section shows that the exponential modulation function has better performance and robustness against noise than the polynomial function when used in the integral observer. A typical active power filter is controlled by a microcontroller or DSP which has a limited computation power. Therefore, a microcontroller and FPGA are selected to implement the algorithm for comparison of the computing times. The basic specifications of the microcontroller and FPGA are listed in Table IV and Table V.

Table III. The error of the modulating function

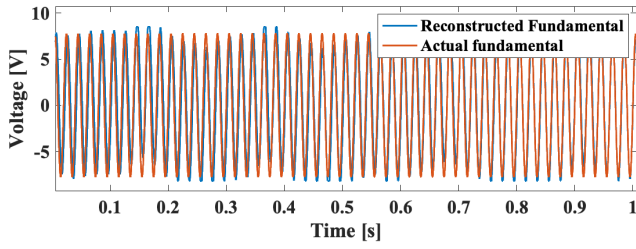| Noise Level (Vpp)	Exponential MF		Polynomial MF		Polynomial MF with band pass filter	
	RMS error(V)	Error boundary(V)	RMS error(V)	Error boundary(V)	RMS error(V)	Error boundary(V)
noiseless	0.3703	2.4594	0.8445	4.6135	0.5865	2.0737
0.26	0.3725	2.5037	1.028	5.1721	0.6002	2.0796
1	0.4082	2.4353	1.0209	5.3679	0.6053	2.0521
2	0.417	2.4221	1.1967	7.7316	0.6019	2.1556
3	0.4077	3.2128	1.4236	9.0187	0.6032	2.2391

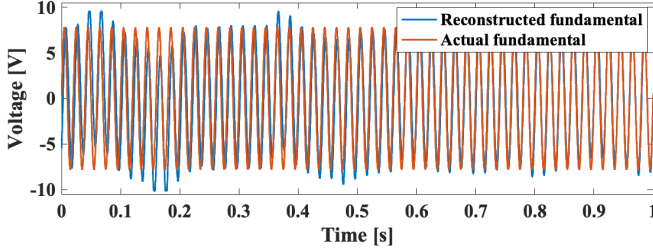Fig. 8a   Actual and reconstructed fundamental by polynomial MF under noiseless condition

Fig. 8b   Actual and reconstructed fundamental by polynomial MF under 2V noise condition
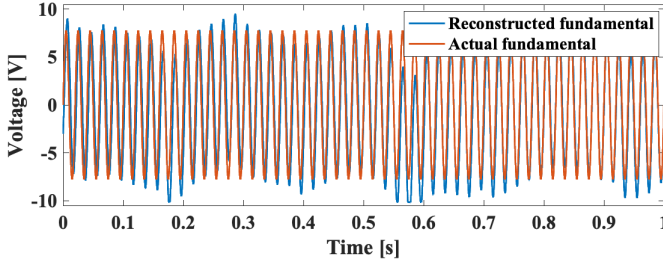

Fig. 8c   Actual and reconstructed fundamental by polynomial MF under 3V noise condition
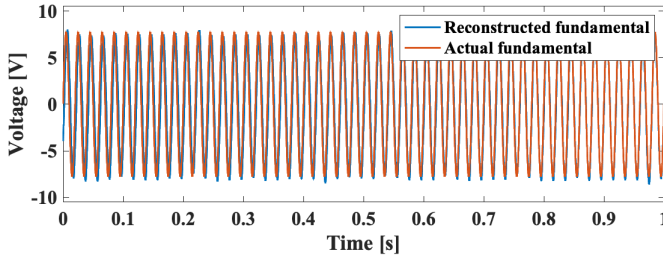

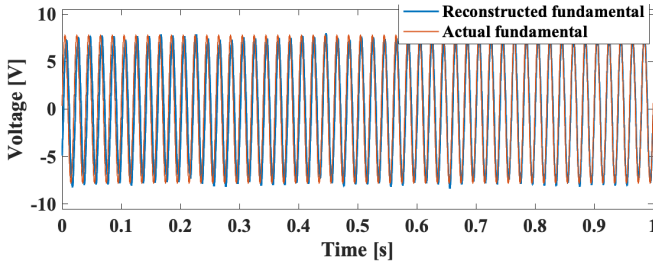Fig. 9a   Actual and reconstructed fundamental by exponential MF under noiseless condition

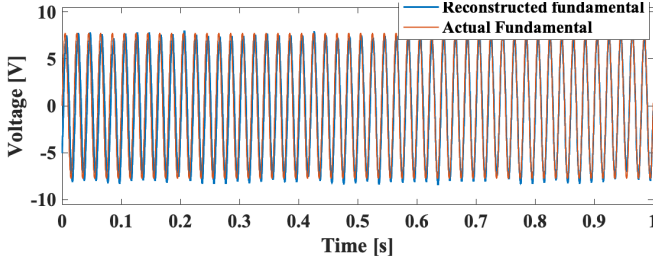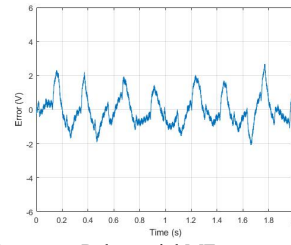Fig. 9b   Actual and reconstructed fundamental by exponential MF under 2V noise condition
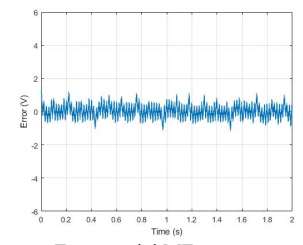

Fig. 9c   Actual and reconstructed fundamental by exponential MF under 3V noise condition
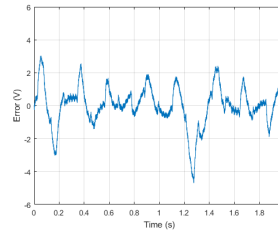

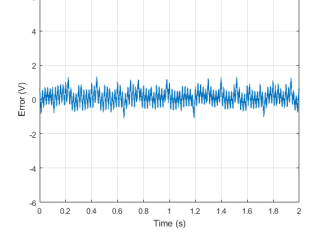(i)   Polynomial MF   (ii)   Exponential MF

Fig. 10a Comparison of error-time series of the (i) polynomial and (ii) exponential MF under Noiseless condition
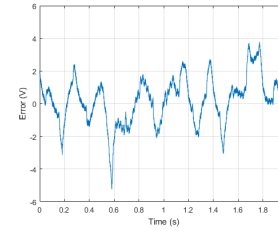

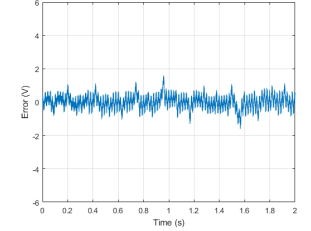(i)   Polynomial MF   (ii)   Exponential MF

Fig. 10b Comparison of error-time series of the (i) polynomial and (ii) exponential MF under 2V noise condition

(i)   Polynomial MF   (ii)   Exponential MF

Fig. 10c Comparison of error-time series of the (i) polynomial and (ii) exponential MF under 3V noise condition

Table IV. Specifications of the microcontroller

MCU model	STM32H7
Max Main Clock frequency	400MHz
Microarchitecture	ARM Cortex-M7F

Table V. Specifications of the FPGA

FPGA Board	Arty S7-50
Look-up Tables (LUTs)	32,600
Flip-Flops	65,200
Block RAM	337.5 KB

Two development boards for the MCU and FPGA have been implemented with the exponential modulation integral observer algorithms. The sampling frequency is set at 10kHz. The periodic distorted waveform generated by the signal generator and the reconstructed fundamental waveform generated by the STM32H7 development board are shown in the Fig. 11. The comparison of the execution times between polynomial and exponential function are listed in Table VI. It is noted that the exponential modulation function requires only 67.5μs, with is well within the sampling time of 100μs of the 10kHz sampling time. This result confirms that such an algorithm can be implemented in MCU. The execution times of the algorithms are about 6μs in FPGA.

Table VI. Computational times on MCU and FPGA

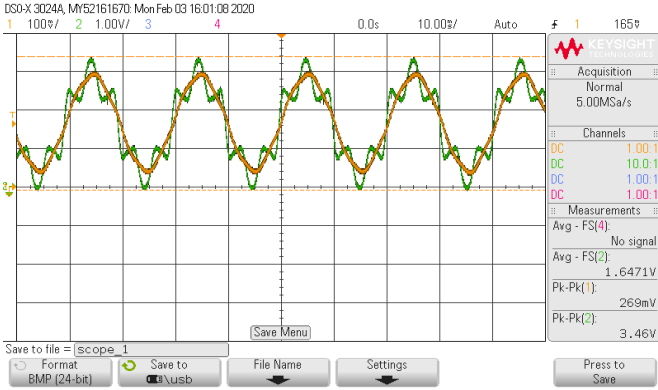| Microcontroller computational time	
Polynomial MF	Exponential MF
22.5µs (<100 µs for 10kHz sampling)	67.5 µs (<100 µs for 10kHz sampling)
FPGA computational time	
Polynomial	Exponential
6.09µs	6.24 µs

Fig. 11 Reconstructed fundamental (orange) and injected harmonic (green) by exponential MF executed by low-cost MCU at a sampling rate of 10kHz

C. Practical comparison of ANF, RDFT and Exp-MF methods in an active power filter application

The hardware setup similar to that of Fig. 1 has been employed to investigate the real-time performance of the proposed algorithm. Fig. 12 shows the photograph of such a setup. In the experiment, a KIKUSUI PBZ40-10 bipolar power supply is to emulate the power grid; a Delta VDF015M21A drive system (VFD) is used as the non-linear load to generate the harmonic current; another KIKUSUI PBZ40-10 bipolar power supply has been set to current mode and acts as the active power filter. Since the bi-polar power supply could only supply a 48V AC voltage, an autotransformer is connected in between the VFD and the bi-polar supply to step-up the voltage to 200V.
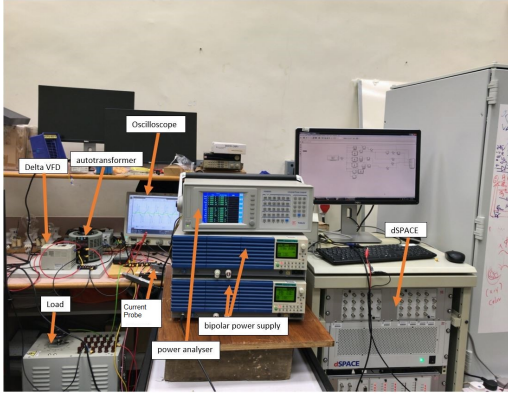

Fig. 12 Hardware setup for active power filter

(i) Steady-state Performance

The non-linear load current drawn by the variable speed drive system is sampled at a frequency of 10kHz. The proposed integral observer with the exponential modulation function (Exp-MF) is compared with the ANF and RDFT methods. For the integral observer, the weighting factors are tuned offline to be $w_1 = 45$, $w_2 = 35$ and $w_3 = 15$. $T_r = T_\Delta = 0.1$. A pair of RDFT filters are employed with the order 0 and 1 for the offset and

fundamental respectively. The ANF is tuned with $\zeta a = 1$ and $\gamma = 10$. Also, the test frequency is extended to a range between 48-52Hz in order to study the robustness of the algorithms for both strong and weak power grids. Details of ANF and RDFT implementations can be found in the appendix of [15].

The total harmonic distortion (THD) of the grid current is calculated by the Voltech PM6000 power analyzer. The data are captured after one minute of operation so as to reduce the error caused by transients.

Fig. 13 shows the mains voltage and the highly distorted input current before harmonic compensation by the active power filter. The total harmonic content is about 50%. The corresponding mains voltage and input current at 50Hz after compensation by the active power filter based on the ANF, RDFT and the Exp-MF methods are shown in Fig. 14, Fig. 15 and Fig. 16, respectively.
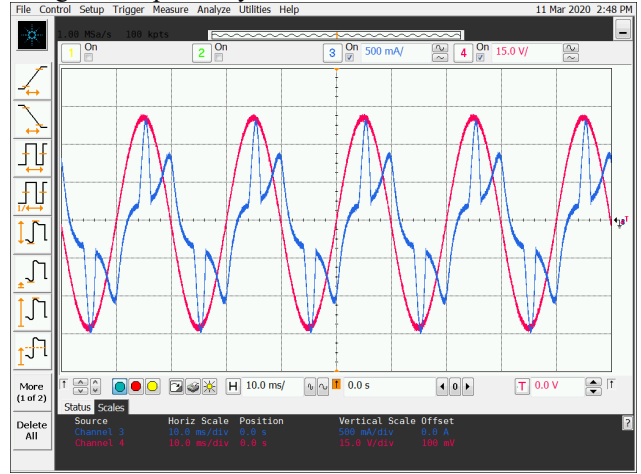

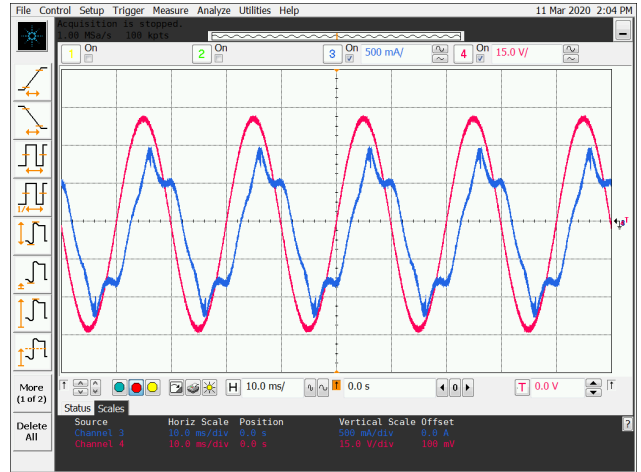Fig. 13 The input current (blue) and power supply voltage (red) without compensation at 50Hz

Fig. 14 The input current (blue), power supply voltage (red) by ANF at 50Hz
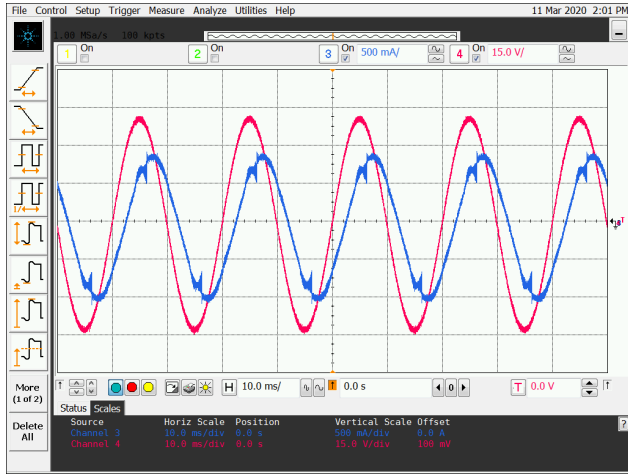
Fig. 15 The input current (Blue), power supply voltage (Red) by RDFT at 50Hz
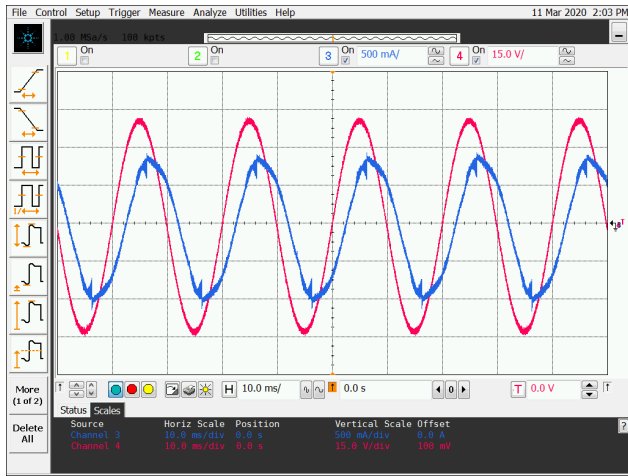

Fig. 16 The input current (blue), power supply voltage (red) by exponential MF at 50Hz

The total harmonic distortion (THD) values of the compensated currents of the three methods under comparison have been measured from 48Hz to 52Hz with an increment of 1Hz. These THD values are tabulated in Table VII. These results show that the performances of both RDFT and the integral observer with the exponential modulation function are comparable and are much better than the ANF method. In this set of tests, the Exp-MF method has a slightly lower THD than RDFT.

Table VII. Grid current THD under different frequencies

Method / Frequency	ANF	RDFT	Exp-MF	Without compensation
48Hz	20.33%	5.86%	5.12%	49.84%
49Hz	19.19%	5.34%	4.97%	49.44%
50Hz	18.47%	5.49%	5.09%	49.40%
51Hz	17.73%	5.25%	5.27%	49.69%
52Hz	17.3%	5.19%	5.49%	50.12%
Averaged THD	**18.60%**	**5.43%**	**5.19%**	**49.70%**

(ii) Dynamic Performance

A normal power grid in Hong Kong and the U.K. should operate between 49.5 to 50.5 Hz and the rate of change of frequency (RoCoF) should not exceed 0.4Hz/s (It would increase to 1Hz/s with more renewable energy connected to the

grid in the future) [16][17]. Under these practical requirements, three representative cases are studied where the fundamental frequency comprises a frequency ramp from 50.5Hz to 49.5Hz with different slopes:

(a)   RoCoF = -0.2Hz/s for a period of T=5s
(b)   RoCoF = -0.4Hz/s for a period of T=2.5s
(c)   RoCoF = -1.0Hz/s for a period of T=1s

A dynamic response test is set up to evaluate the performance of the exponential MF and the RDFT methods. A dSPACE system is used to control a bipolar power supply to generate a distorted current of the shape shown in Fig. 7 for the three cases with specified RoCoF values. The exponential-MF and RDFT methods are implemented to derive the fundamental component of the distorted current. To compare their transient performance, the root-mean-square (RMS) estimation errors of both methods within the transient period are evaluated by:

$$\sqrt{\frac{\sum(i_n - i_n^*)^2}{T}}$$

where i_n and i_n* are the ideal and sampled current values, respectively. For the three cases, the largest error boundaries (which is the maximum error minus the minimum error) are also recorded. These results are tabulated in Table VIII. It can be shown that the exponential MF method has smaller RMS errors and error boundaries than the RDFT method in all of the three cases.

Table VIII   Comparison of Dynamic Performance of Exponential MF and RDFT for a range of RoCoF

RoCoF (Hz/s)	Exp-MF RMS Error (A)	RDFT RMS Error (A)	Exp-MF Error boundary (A)	RDFT error boundary (A)
0.2	0.1191	0.1103	0.4698	0.5013
0.4	0.2037	0.2879	1.0176	1.3455
1	0.5009	0.7042	1.956	2.4309

For illustrative purposes, the error signals of RDFT and exponential MF method in case (c) are depicted in Fig. 17, where the scale of both methods is the same. The results verify the superior performance of the proposed estimation scheme.
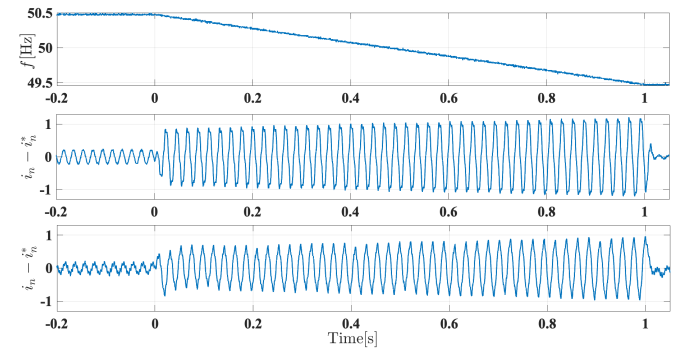

Fig.17 The estimation error signal of the MF exp and RDFT during a frequency ramp change. Top: fundamental frequency. Middle: fundamental signal estimation error of RDFT. Bottom: fundamental signal estimation error of Exp-MF

VI. Conclusion

An integral-observer-based modulation function was recently reported to be a fast and effective solution in detecting the fundamental and thus the total harmonic content of a periodic waveform. The novel contributions of this paper include a thorough theoretical analysis, a mathematic proof and practical verification that an integral observer based on an exponential modulation function will offer better robustness against noise and aliasing issues than that based on a polynomial modulation function. The computational times obtained in real-time implementation confirm that the proposed exponential modulation integral observer can be used in low-cost MCU for real-time operation. The proposed method has been practically compared with the ANF and RDFT methods in a practical real-time application of an active power filter. The total harmonic distortion values confirm the good performance of the proposed method. Under a range of rate of change of frequency in an a.c. power system, the proposed method provides a re-constructed fundamental component from a distorted waveform with smaller error and error boundary than the RDFT method. Thus, the proposed method can provide good performance in both fixed and variable frequency situations. The study advances the integral observer technology for identifying the fundamental and hence the total harmonic content by introducing a new exponential modulation function to enhance the integral observer's robustness against noise and mitigate the aliasing issues. Its ability to withstand noise in the sampled signal has been theoretically analyzed and proved, and also experimentally verified. The exponential modulation function integral observer offers the combined advantages of fast computation and high robustness. It is a feasible option for adoption in grid-tied power inverters that require the information of the fundamental and harmonic content in real time for control purposes.

References

[1] John Douglas, "Quality of Power In The Electronics Age", *IEEE Power Engineering Review*, Vol: PER-6, Iss: 3, pp. 5 – 8, Year: 1986.

[2] H. Akagi, "Trends in active power line conditioners," *IEEE Trans. Power Electron*., vol. 9, (3), pp. 263–268, May 1994

[3] W.M. Grady ; M.J. Samotyj ; A.H. Noyola, "Survey of active power line conditioning methodologies", IEEE Trans on Power Del., Vol:5 (3), pp. 1536 – 1542, 1990

[4] H. Akagi, "Active harmonic filters," Proc. IEEE, vol. 93, no. 12, pp. 2128–2141, Dec. 2005

[5] L. Asiminoaei, F. Blaabjerg, and S. Hansen, "Detection is key - Harmonic detection methods for active power filter applications," in *IEEE Industry Applications Magazine*, vol. 13, no. 4, pp. 22-33, July-Aug. 2007

[6] B. McGrath, D. Holmes, and J. Galloway, "Power converter line synchronization using a discrete fourier transform based on a variable sample rate," *IEEE Trans. on Power Electron*., vol. 20, no. 4, pp. 877–884, 2005.

[7] S. Gonzalez, R. Garcia-Retegui, and M. Benedetti, "Harmonic computation technique suitable for active

power filters," *IEEE Trans. on Ind. Electron*., vol. 54, no. 5, pp. 2791–2796, 2007.

[8] E. Jacobsen and R. Lyons, "The sliding DFT," *IEEE Signal Process. Mag.*, vol. 20, no. 2, pp. 74–80, 2003.

[9] E. Jacobsen and R. Lyons, "An update to the sliding DFT," *IEEE Signal Process. Mag*., vol. 21, no. 1, pp. 110–111, 2004.

[10] X. Yuan, W. Merk, H. Stemmler, and J. Allmeling, "Stationary-frame generalized integrators for current control of active power filters with zero steady-state error for current harmonics of concern under unbalanced and distorted operating conditions*," IEEE Trans. Ind. Appl*., vol. 38, no. 2, pp. 523–532, 2002.

[11] V. M. Moreno, M. Liserre, A. Pigazo, and A. D. Aquila, "A comparative analysis of real-time algorithms for power signal decomposition in multiple synchronous reference frames," *IEEE Trans. on Power Electron*., vol. 22, no. 4, pp. 1280–1289, 2007.

[12] D. Yazdani, A. Bakhshai, G. Joos, and M. Mojiri, "A real-time three-phase selective-harmonic-extraction approach for grid-connected converters," *IEEE Trans. on Ind. Electron*, vol. 56, no. 10, pp. 4097–4106, 2009.

[13] H. Kim and H. Akagi, "The instantaneous power theory based on mapping matrices in three-phase four-wire systems," in *IEEE Proc. of Power Conversion Conference*, pp. 361–366, 1997

[14] G. Pin, B. Chen, and T. Parisini, "Robust deadbeat continuous-time observer design based on modulation integrals," *Automatica*, Vol: 107, 2019.

[15] B. Chen, G. Pin, W. M. Ng, T. Parisini, and S.Y. Ron Hui, "A Fast-Convergent Modulation Integral Observer for Online Detection of the Fundamental and Harmonics in Grid-Connected Power Electronics Systems", *IEEE Trans. on Power Electron*, Vol:32, Iss.4 , pp: 2596 – 2607, 2017

[16] National Grid. (2020), The Grid Code. [Online]. Available:https://www.nationalgrid.com/sites/default/files/documents/8589935310-Complete%20Grid%20Code.pdf

[17] National Grid. (2014). System Operability Framework 2014.[Online].Available:https://www.nationalgrideso.com/document/63446/download

V. Appendix

A. Periodic rescaling strategy

To introduce the rescaling strategy, let us now consider the time-shifted counterpart of the modulation integral (15)

$$v_{\phi h}(t|t_0) = \int_{t_0}^{t} \phi_h^{(3)}(\tau - t_0)\, i(\tau)$$
$$+ \omega^2 \phi_h^{(1)}(\tau - t_0)i(\tau)\, d\tau \qquad (A.1)$$

where t_0 is a time instant different from 0. On this occasion, a time-shifted version of (14) can be obtained

$$z(t) = \Gamma(t - t_0)^{-1} V_\phi(t|t_0). \qquad (A.2)$$

Define two positive scalars T_Δ and T_r, dividing the time span into successive segments terminated at

$$t_k = T_\Delta + (k+1)T_r, \quad k = 0,1,\cdots$$

Noting that (A.2) holds for any generic t_0, the following two equations both hold, for all $t > t_k - T_\Delta, k = 1,2,\cdots$.

$$z(t) = \Gamma(t - (t_k - T_\Delta))^{-1}V_\phi(t|t_k - T_\Delta)$$
$$z(t) = \Gamma\big(t - (t_{k-1} - T_\Delta)\big)^{-1}V_\phi(t|t_{k-1} - T_\Delta) \qquad (A.3)$$

It is worth to point out that the vector signal $V_\phi(t|t_k - T_\Delta)$ contains the information collected in the time-window $[t_k - T_\Delta, t]$, while $V_\phi(t|t_{k-1} - T_\Delta)$ contains information collected in a longer time-window $[t_{k-1} - T_\Delta, t]$. Referring the two identities in (A.3), it is possible to establish an algebraic relation between $V_\phi(t|t_k - T_\Delta)$ and $V_\phi(t|t_{k-1} - T_\Delta)$ that permits to discard old information carried by the data processed in the interval $[t_{k-1} - T_\Delta, t_k - T_\Delta]$. Therefore, for $t = t_k$, according to (A.3), it holds that

$$\Gamma(t_k - (t_k - T_\Delta))^{-1}V_\phi(t_k|t_k - T_\Delta) = \Gamma\big(t_k - (t_{k-1} - T_\Delta)\big)^{-1}V_\phi(t_k|t_{k-1} - T_\Delta),$$

which can be reformed as

$$V_\phi(t_k|t_k - T_\Delta) = \Gamma(T_\Delta)\Gamma(T_r + T_\Delta)^{-1}V_\phi(t_k|t_{k-1} - T_\Delta).$$

That is to say, the vector $V_\phi(t_k|t_k - T_\Delta)$ can be computed from the vector $V_\phi(t_k|t_{k-1} - T_\Delta)$ through a simple algebraic rescaling, which is smooth as a result of (A.3). For clarification, T_r is the time between two rescaling events, while T_Δ represents the length of the equivalent integration window after each operation.

To ensure the error signal is downscaled after each resetting instant, the constant rescaling gain $|\Gamma(T_\Delta)\Gamma(T_r + T_\Delta)^{-1}|$ needs to be sufficiently small (fulfilled by suitably designed T_r and T_Δ). Readers can refer to [14] for detailed characterization.